Liquid Crystals
Publication details, including instructions for authors and subscription information:
http://www.informaworld.com/smpp/title~content=t713926090

Characterisation and mesomorphic behaviour of new aliphatic-aromatic azomethines containing ester groups

Agnieszka Iwan[a]; Damian Pociecha[b]; Andrzej Sikora[a]; Henryk Janeczek[c]; Marcin Wegrzyn[c]
[a] Electrotechnical Institute, Division of Electrotechnology and Materials Science, Wroclaw, Poland [b] Department of Chemistry, University of Warsaw, Warsaw, Poland [c] Centre of Polymer and Carbon Materials, Polish Academy of Sciences, Zabrze, Poland

Online publication date: 10 December 2010

To cite this Article Iwan, Agnieszka , Pociecha, Damian , Sikora, Andrzej , Janeczek, Henryk and Wegrzyn, Marcin(2010) 'Characterisation and mesomorphic behaviour of new aliphatic-aromatic azomethines containing ester groups', Liquid Crystals, 37: 12, 1479 — 1492
To link to this Article: DOI: 10.1080/02678292.2010.530297
URL: http://dx.doi.org/10.1080/02678292.2010.530297

Liquid Crystals,
Vol. 37, No. 12, December 2010, 1479–1492

Taylor & Francis
Taylor & Francis Group

Characterisation and mesomorphic behaviour of new aliphatic–aromatic azomethines containing ester groups

Agnieszka Iwan[a]*, Damian Pociecha[b], Andrzej Sikora[a], Henryk Janeczek[c] and Marcin Wegrzyn[c]

[a]*Electrotechnical Institute, Division of Electrotechnology and Materials Science, Wroclaw, Poland;* [b]*Department of Chemistry, University of Warsaw, Warsaw, Poland;* [c]*Centre of Polymer and Carbon Materials, Polish Academy of Sciences, Zabrze, Poland*

(*Received 31 March 2010; final version received 5 October 2010*)

Two series of novel symmetrical azomethines prepared by the condensation of 4,4′-(butane-1,4-diylbis(oxy)) bis(butane-4,1-diyl)bis(4-aminobenzoate) (**PBBA470**) and 5,10,15,20,25,30,35,40,45,50,55,60-dodecaoxatetrahexacontane-1,64-diylbis(4-aminobenzoate) (**PBBA 1200**) with a range of aldehydes have been characterised by ^{1}H and ^{13}C nuclear magnetic resonance, Fourier transform infrared and UV–Vis spectroscopy. Current–voltage measurements were performed using a device comprising indium–tin oxide/compound/Alq_3/Al. The effect of rod length and the nature of the terminal chains on the thermal and mesomorphic behaviour of these materials were investigated by differential scanning calorimetry, polarising optical microscopy and wide- and small-angle X-ray diffraction. Additionally, the compounds were studied using various atomic force microscopy techniques, including mode and phase imaging, and measurements based on local contrast force–distance curves and roughness, together with skew and kurtosis, are presented.

Keywords: imines; azomethines; oligomers; liquid crystals; optical properties; electrical properties

1. Introduction

Liquid crystal (LC) oligomers, such as dimers, trimers, tetramers, etc., consist of molecules containing two or more mesogenic units, usually interconnected by alkyl chains. Compounds of this type have been widely investigated [1–27] since they exhibit different properties in comparison with low-molecular mass mesogens, and are referred to as pre-organised systems [4]. The relationship between molecular shape and macroscopic phase behaviour continues to be extensively investigated. In previous studies we have investigated the optical (absorption, photoluminescence and thermoluminescence) and electrical (current–voltage) properties of a range of symmetrical and non-symmetrical azomethines [28–35]. Most recently, we have described the thermal and opto-electrical properties (absorption, photoluminescence and thermoluminescence) of bis[4-((4-biphenylomethyleno)amino) benzoate] 4,4′-(butane-1,4-diylbis(oxy)bis(butane-4,1-diyl)bis(4-(biphenyl-4-ylmethyleneamino)benzoate) [35]. This imine exhibited SmA and SmB mesophases, confirmed by DSC, POM and X-ray diffraction.

In our opinion it is important to employ a combination of thermal, optical and electrical measurements to identify potential applications for imines of this nature, making use of their thermal stability and solution processability. For this reason, in the present study we have investigated two series of azomethines prepared from 4,4′-(butane-1,4-diylbis(oxy))bis(butane-4,1-diyl) bis(4-aminobenzoate (**PBBA470**) and 5,10,15,20,25,30,35,40,45,50,55,60-dodecaoxatetrahexacontane-1,64-diyl bis(4-amino benzoate) (**PBBA1200**) condensed with a variety of aldehydes. The influence of rod length and the nature of the terminal chains on the properties of these materials have been assessed in detail using the following techniques:

- thermal: polarising optical microscopy (POM) and differential scanning calorimetry (DSC);
- optical: ultraviolet–visible (UV–Vis), Fourier transform infrared (FTIR) and ^{1}H and ^{13}C nuclear magnetic resonance (NMR) spectroscopy;
- electrical: current–voltage (*I–V*); and
- structural: atomic force microscopy (AFM) and X-ray diffraction (XRD).

In this article we present the thermal, optical and structural characterisation of a series of thermotropic π-conjugated calamitic LC azomethines. The properties of symmetrical azomethines based on **PBBA1200** have not previously been reported.

2. Results and discussion

2.1 Synthesis and characterisation

The two series of azomethines described were prepared from **PBBA470** and **PBBA1200** by melt condensation

*Corresponding author. Email: a.iwan@iel.wroc.pl

ISSN 0267-8292 print/ISSN 1366-5855 online

DOI: 10.1080/02678292.2010.530297
http://www.informaworld.com

with a range of aldehydes at 170°C. All the compounds are new, apart from **PBBA470C**, which was the subject of an earlier study [35], and in the present investigation was used as a reference material. Other than **PBBA470B,** all the compounds were soluble at room temperature in chloroform, dimethylacetamide (DMA) or dimethylformamide (DMF). The azomethines were characterised by FTIR, and ^{1}H and ^{13}C NMR spectroscopy.

The synthetic pathways and the chemical structures of the azomethines are illustrated in Figures 1 and 2. Their spectroscopic and molecular characteristics are summarised in the Experimental section. The spectral data were in accordance with the expected formula.

The absence of residual amino (NH_2) and aldehyde (CHO) groups and the appearance of peaks characteristic of azomethine bonds (HC=N) were confirmed by FTIR and NMR spectroscopy. The spectra have been used to confirm the purity and molecular structure of the final products. In Table 1 ^{1}H and ^{13}C NMR NMR and FTIR parameters attributable to the characteristic bonds of the target imines are summarised.

In the Experimental section, NMR data for all the imines investigated are presented. In particular, signals in the range 151–161 ppm were present in the ^{13}C NMR spectra of all the compounds, and confirm the presence of the azomethine group. The changes in the shift observed by modifying the chemical constitution of the aldehyde are clearly apparent. For example, in **PBBA470C** the presence of two phenyl rings resulted in a downward shift relative to **PBBA470A** in the line related to the azomethine carbon atom. On the other hand, the presence of thiophene rings in **PBBA470D** produced a small downward shift in the azomethine line relative to **PBBA470A**, and an upward shift in comparison with the other imines. However, for the imines obtained from **PBBA1200** and different aldehydes such as 4-biphenyl carboxaldehyde (**PBBA1200A**) and 4-(4,4,5,5,6,6,7,7,8,8,9,9,10,10,11,11,11-heptadecafluoroundecyloxy)benzaldehyde (**PBBA1200B**), no shift in the line related to the azomethine carbon atom was observed. Given the diamine structure present in imines **PABA470** and **PABA1200,** it was significant that no difference in the position of the imine bond in the ^{13}C NMR spectra could be observed (Table 1).

Most signals were assigned based on the well-known ^{1}H NMR chemical shift resulting from electron shielding or de-shielding of the hydrogen nuclei by inductive effects, or from the diamagnetic anisotropy, caused by various neighbouring groups. In the Experimental section, ^{1}H NMR data for all the compounds investigated are summarised, together with the NMR peaks observed. For example, in the case of **PBBA1200B,** which contained perfluorinated chains, the signal from the imine group was observed at a higher frequency (8.37 ppm), whereas the presence of thiophene rings in **PBBA470D** caused a significant upward shift in the imine ^{1}H NMR signal, to 8.57 ppm.

The presence of imine groups was also confirmed by FTIR spectroscopy, and in each case the absorption band characteristic of HC=N deformation was detected. The exact position of the band varied within the range 1605–1627 cm^{-1}, shifted to higher wave numbers in the case of compounds **PBBA1200A**, **PBBA1200B** and **PBBA470A**. In addition to the HC=N stretching band, a band at about 1590 cm^{-1} was present and could be assigned to C=C stretching in the aromatic ring. Absorption at shorter wavelengths, around 1605 cm^{-1}, was observed with the imine containing thiophene rings **PBBA470D** (see Table 1). Large differences were not observed in the position of the azomethine band in the FTIR spectra, given the nature of the diamine structure. For **PBBA470B**, an imine containing two hydroxyl groups, the HC=N stretching band was present at

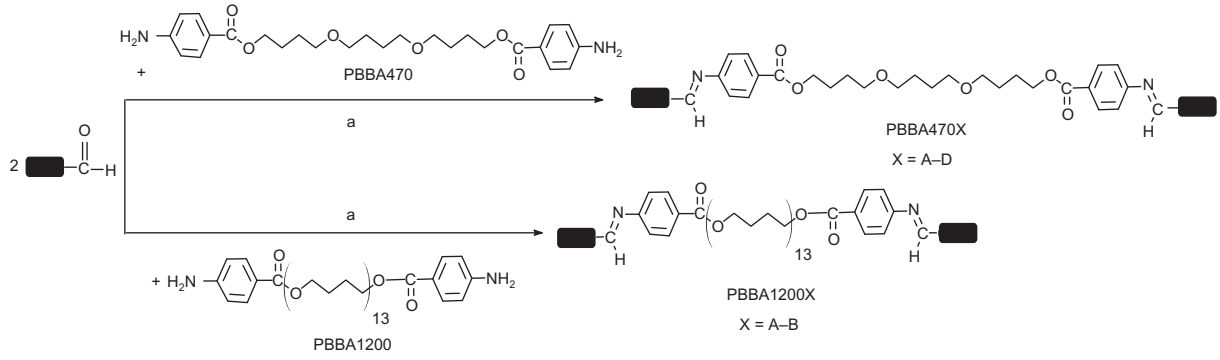

Figure 1. Synthetic route to the imines. Note: a = 170°C, 24 h.

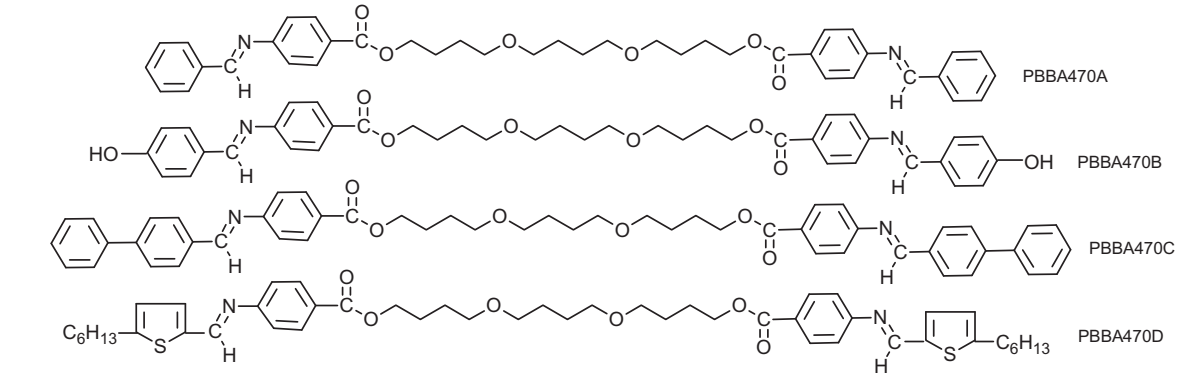

(a)

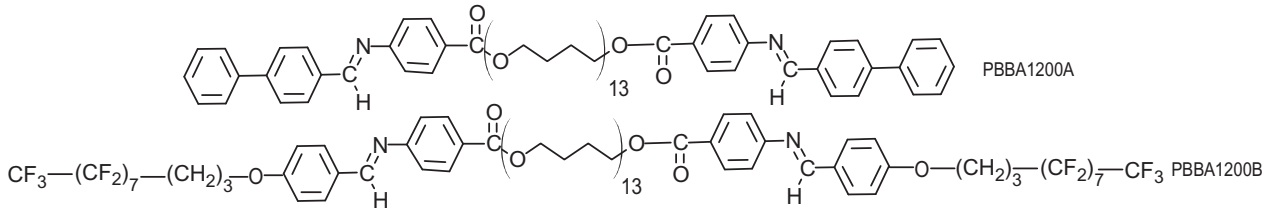

(b)

Figure 2. Structure of the imines synthesised from (a) **PBBA470** and (b) **PBBA1200**.

Table 1. Selected bands detected in ^{1}H and ^{13}C NMR and FTIR spectroscopy.

	^{1}H NMR (ppm)			^{13}C NMR (ppm)		FTIR (cm^{-1})	
Compound	$\delta_{CH=N}$	$\delta_{HAr-C(O)O}$	$\delta_{CH2-C(O)O}$	$\delta_{CH=N}$	$\delta_{O-C=O}$	**–O–C=O**	**CH=N**
PBBA470A	8.45	8.05 – 8.15	4.26	150.7	166.7	1695	1627
PBBA470B	–*	–*	–*	–*	–*	1704	1620
PBBA470C	8.47	8.07 – 8.10	4.36	161.2	166.4	1712	1625
PBBA470D	8.57	8.10	4.20 – 4.50	153.5	166.0	1711	1605
PBBA1200A	8.48	8.07	4.26 – 4.38	161.2	166.7	1709	1626
PBBA1200B	8.37	8.05 – 8.08	4.26 – 4.36	161.0	166.3	1710	1626

Note: *Insoluble in chloroform.

about 1620 cm^{-1}, a shift to lower wavelengths by comparison with **PBBA470A** (see Table 1).

It is interesting that all the imines investigated were soluble in chloroform and DMA, apart from **PBBA470B,** which contained two hydroxyl groups *para* to the imine bonds (see Figure 2).

The glass transition temperature (T_g) of the imines was determined by DSC, with heating scans at 10°C min^{-1}. All the compounds showed clear glass transitions (see Figure 3). The highest glass transition temperature was shown by **PBBA470C** and the lowest by **PBBA1200B**. In general, compounds prepared from the diamine **PBBA1200** exhibited lower T_g than those from **PBBA470**. This can be explained by the increased length of the aliphatic portion of the diamine.

Taking **PBBA470C**, **PBBA470D**, **PBBA120A** and **PBBA1200B** as representative, dilute solutions were prepared in chloroform and cast on quartz slides for UV–Vis assessment (see Experimental). All the compounds exhibited one clear absorption peak in the range 274–311 nm at room temperature, attributable to π–π^* transitions. No difference was observed between the maximum of the absorption spectra of compounds **PBBA1200A** and **PBBA1200B**. On the other hand, the incorporation of the thiophene group in the azomethine structure (**PBBA470D**), or two phenyl rings in **PBBA470C,** caused a red shift in the absorption band, to 304 nm and 311 nm, respectively. This behaviour confirmed the greater conjugation in the compounds, **PBBA470C** and **PBBA470D**, than in the azomethines, **PBBA1200A** and **PBBA1200B**, and caused a 30–37 nm red shift in the absorption maximum of **PBBA470C** and **PBBA470D** by comparison with **PBBA1200A** and **PBBA1200B**. Given

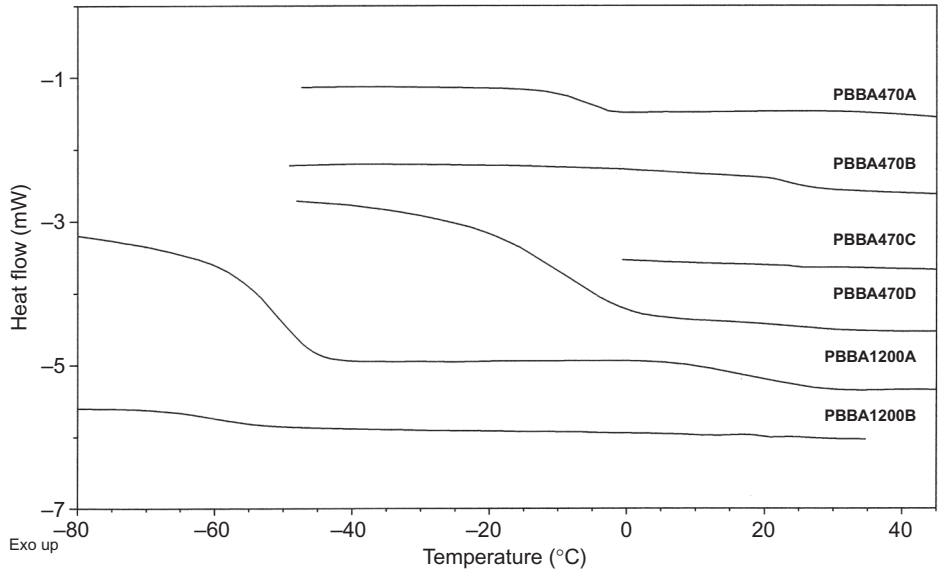

Figure 3. T_g of the imines investigated (heating scan at 10°C min^{-1}).

the diamine structures, we observed differences in the position of the absorption bands of the azomethines investigated. The maximum of the absorption band of **PBBA470C** occurred at 311 nm at room temperature and showed a 36 nm red shift in comparison with the absorption maximum of **PBBA1200A**.

2.2 Current–voltage characteristics

I–V measurements were performed using an indium–tin oxide (ITO)/imine/ aluminium tris(8-hydroxyquinoline) (Alq_3)/Al device. The imines **PBBA470C**, **PBBA470D**, **PBBA470A** and **PBBA1200A** were used as representative examples. The azomethine solution (1 w/v% in dichloroethane) was spun-cast on an ITO-covered glass substrate at room temperature to produce a thin hole transporting layer (HTL). Residual traces of solvent were removed by heating the film in a vacuum. The green-emitting Alq_3 layer was vacuum deposited on the HTL layer at a base pressure of *ca.* 10^{-6} Torr, followed by deposition of an aluminium electrode at a similar vacuum. *I–V* curves of ITO/**PBBA470C**/Alq_3/Al devices have been published previously [16] and in the present paper are used for reference purposes. The construction of the device is illustrated in Figure 4(a), and *I–V* curves of the devices ITO/**PBBA470C**/Alq_3/Al, ITO/**PBBA470D**/Alq_3/Al, ITO/**PBBA470A**/Alq_3/Al and ITO/**PBBA1200A**/Alq_3/Al determined at room temperature are shown in Figure 4(b).

The turn-on voltage of the device ITO/**PBBA 470C**/Alq_3/Al was observed at about 3 V at room temperature in the dark. The corresponding turn-on voltages for ITO/**PBBA470D**/Alq_3/Al, ITO/**PBBA 470A**/Alq_3/Al and ITO/**PBBA1200A**/Alq_3/Al were around 16 V, 7 V and 7 V, respectively.

In addition, *I–V* curves for the ITO/**PBBA1200A** /Alq_3/Al device with different thicknesses of the **PBBA1200A** layer were determined at room temperature, and are shown in Figure 4(c). The turn-on voltage of this device with an active layer of thickness 150 nm was observed at about 7 V at room temperature, and small differences were seen on increasing the thickness from 150 to 250 nm. For a film thickness of about 150 nm the current increased rapidly with increasing applied voltage, but at thicknesses of 200 to 250 nm the turn-on voltage remained constant at around 8 V.

This behaviour demonstrated the influence of the structure of this group of azomethines, particularly the nature of the terminal groups, on their electrical properties. The effect on *I–V* characteristics strongly suggested differences in the planarity and conformation of these compounds in the films.

2.3 AFM study

The influence of the length of the aliphatic core (**PBBA470C** and **PBBA1200A**) on the surface morphology of the materials was investigated. Films were cast on glass, after dissolving the compounds in chloroform at room temperature to form a homogeneous solution. Residual solvent in the film was removed by heating. Figure 5 shows the AFM images obtained for selected imines, and very interesting morphologies are revealed. These are characteristic of systems capable of forming organised supramolecular structures, and the linearity of the imines with shorter ((–O–CH_2)$_3$–) and

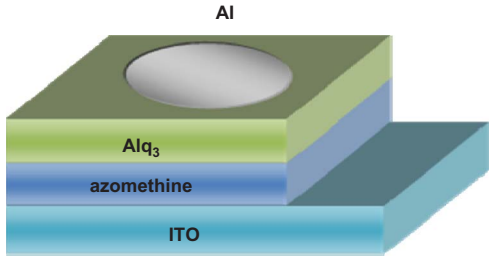

(a)

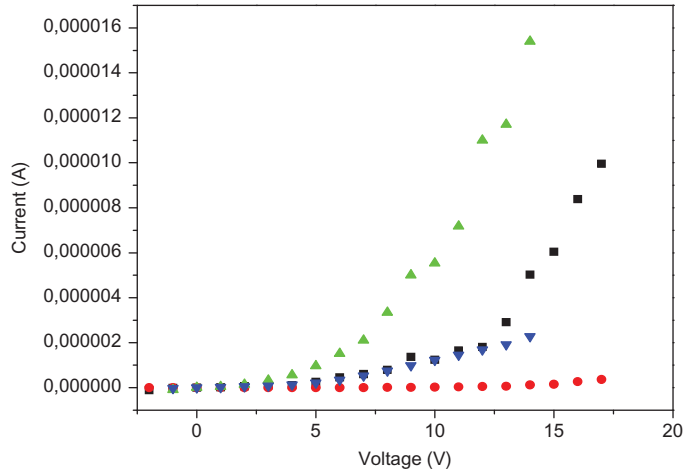

(b)

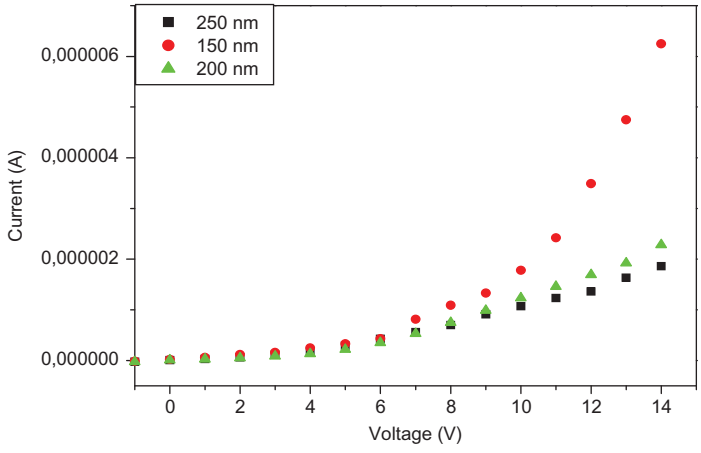

(c)

Figure 4. (a) Schematic of the device used in the study; (b) *I–V* curves of the systems ITO/**PBBA470C**/Alq_3/Al (▲), ITO/**PBBA470D**/Alq_3/Al (●), ITO/**PBBA470A**/Alq_3/Al (■) and ITO/**PBBA1200A**/Alq_3/Al (▼); (c) *I–V* curves of the system ITO/**PBBA1200A**/Alq_3/Al at different thickness of the active layer (colour version online).

longer ($(–O–CH_2)_{13}–$) oxyaliphatic spacers between the mesogenic units was seen to be different. AFM images of **PBBA470C** showed some organisational features, clearly seen in the inclination transformation shown in Figure 5.

On the other hand, it is easy to see the influence of molecular weight on surface morphology. The most highly organised supramolecular structures were observed with **PBBA1200A,** which had a higher molecular weight than **PBBA470C**.

When the topography was measured one could obtain certain data describing the properties of the surface. The quantities most commonly described are roughness average (Ra) and the root mean square

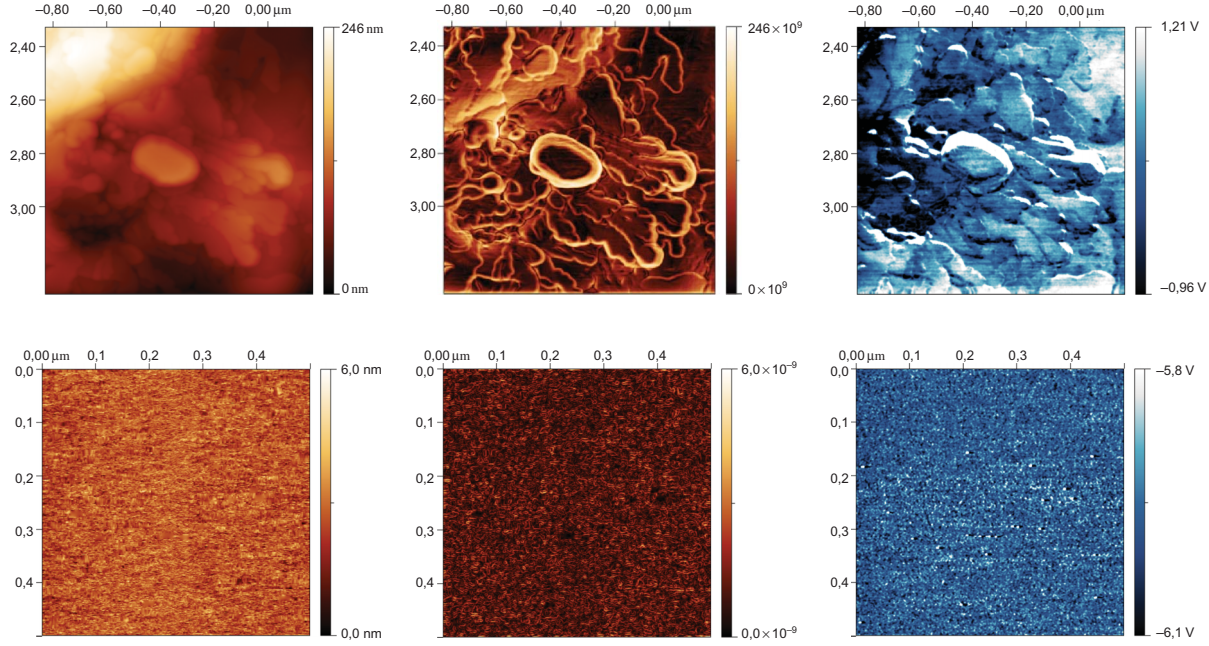

Figure 5. AFM images of **PBBA470C** (upper) and **PBBA1200A** (lower); topography processed (left), inclination transformation (centre) and phase imaging (right) (colour version online).

Table 2. Surface parameters of selected azomethines.

	Surface statistics				
Code	Ra (nm)	RMS (nm)	Skew	Kurtosis	Surface area ratio
PBBA470C	36.20	50.00	1.59	2.08	1.1333
PBBA1200A	0.41	0.53	0.06	0.43	1.1405

average (RMS) of peaks and valleys in the surface profile. It is useful, however, to include additional values such as skew (the unbalance of height distribution maximum) and kurtosis (the distribution of the width of peaks in relation to height). These quantities are presented in Table 2 for the two surfaces studied.

The results obtained using AFM techniques confirmed that these are powerful and valuable tools for micro- and nanoscale analysis of surface properties. Further refinement of these techniques will increase the information we have, both qualitative and quantitative, of such surfaces.

2.4 Thermal behaviour

In order to establish their mesomorphic behaviour, the imines were studied using DSC and POM. The DSC scans are shown in Figure 6.

The transition temperatures and associated enthalpy change of the imines determined by DSC are summarised in Table 3.

Of the six azomethines investigated, only two (**PBBA470C** and **PBBA1200B**) exhibited mesomorphic behaviour. This confirmed the role of the rods and terminal chains in promoting the mesomorphic properties of the imines. The azomethine **PBBA470B** had a melting point about 198°C. The compounds investigated were polydisperse, as can be seen from their DSC traces and optical textures.

PBBA470A showed two endothermic peaks during the first and second heating scans, conducted at 2.5 deg min^{-1}. On cooling from the isotropic phase to room temperature two exothermic peaks appeared, at 15.4 and 20.7°C, with associated enthalpy changes of 0.46 and 0.42 J g^{-1}, respectively. On the other hand, **PBBA470D** showed during the heating scan at 1 deg min^{-1} three peaks, at 32.8, 51.9 and 101°C. However, subsequent heating of the sample, at 10 deg min^{-1}, showed only two endothermic peaks, at 33.9 and 58.3°C, with associated enthalpy changes of 0.38 and 0.37 J g^{-1}, respectively. The transitions observed were monotropic; no peaks were observed during cooling.

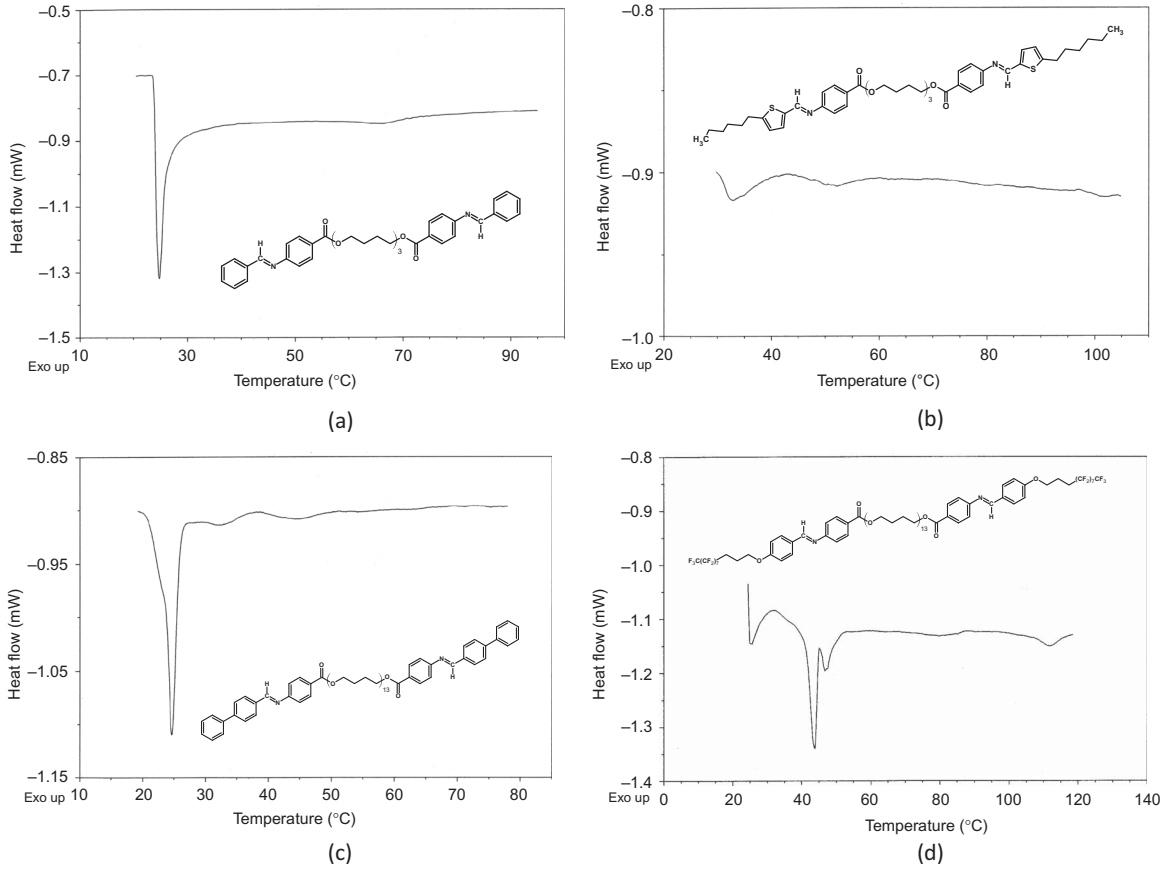

Figure 6. DSC traces of: (a) **PBBA470A** (heating rate, 2.5 deg min^{-1}), (b) **PBBA470D** (heating rate, 1 deg min^{-1}), (c) **PBBA1200A** (heating rate, 0.8 deg min^{-1}), (d) **PBBA1200B** (heating rate, 1.5 deg min^{-1}).

Table 3. Phase transition temperatures (°C) determined by DSC, with enthalpy values (J g^{-1}).

Compound	DSC, Temp.(°C) (ΔH (J g^{-1}))
PBBA470A*	Cr 21.8 (7.87), I 64.6 (5.11)
PBBA470A*	Cr 24.7 (8.54), I 66.4 (1.27)
PBBA470B	198.4 (6.13)
PBBA470C**	"cold" Cr 88.9 (51.8), Sm B 126.1 (56.5), Sm A 149.8 (8.7), I
PBBA470D**	Cr 32.8 (0.94), Cr1 51.9 (0.42), I 101.0 (0.06)
PBBA470D***	Cr 33.9 (0.38), Cr1 58.3 (0.37)
PBBA1200A****	Cr 24.6 (5.17), Cr1 33.1 (0.20), Cr2 44.7 (0.54), I 63.8 (0.14)
PBBA1200A****	"cold" Cr 1.6 (1.56), Cr1 30.9 (0.87), I 62.2 (0.67)
PBBA1200B*****	Cr 43.6, 46.9 (3.05), Sm 79.9 (0.42), I 111.7 (0.63)
PBBA1200B*****	Cr 44.4, 49.0 (2.07), Sm 89.9 (0.25), I 109.4 (0.20)

Notes: *First and second heating scan at 2.5 deg min^{-1}, ** heating 1 deg min^{-1}, *** heating 10 deg min^{-1}, **** heating 0.8 and 10 deg min^{-1}, ***** first and second heating scan at 5 deg min^{-1}

PBBA1200A exhibited four endothermic peaks during the first heating scan at 0.8 deg min^{-1} (Table 3). Moreover, during the next heating at 10 deg min^{-1}, **PBBA1200A** exhibited two endotherms, at 30.9 and 62.2°C (ΔH = 0.87 and 0.67 J g^{-1}), along with an exothermic peak at 1.6°C (1.56 J g^{-1}). It is interesting that for the azomethines obtained from 4-biphenyl carboxaldehyde, so called "cold" crystallisation was observed during the heating of the sample (see Table 3).

During the first and second heating scans at 5 deg min^{-1}, **PBBA1200B** exhibited four endothermic peaks, shown in Table 3. On cooling from the isotropic phase to room temperature, two exothermic peaks appeared at 50.5 and 80.0°C, with associated enthalpy changes of 1.21 and 1.09 J g^{-1}, respectively.

PBBA470C exhibited the following phase transitions: crystal to mesophase (Cr/M), mesophase to mesophase (M/M1) and mesophase to isotropic (M1/I), whereas **PBBA1200B** exhibited two enantiotropic transitions: crystal to mesophase (Cr/M) and mesophase to isotropic (M/I).

PBBA470C exhibited two smectic mesophases (SmA and SmB) [35]. Compounds **PBBA470A** and **PBBA470D** behaved differently and only isotropic phases were observed.

A separate approach to tuning thermotropic properties involves the introduction of terminal chains of different polarity. Increasing the number of phenylene rings also influences the presence of mesophases (compare **PBBA470A** and **PBBA470C**).

Imines prepared from the diamine **PBBA1200** occupied a structural position intermediate between small compounds and polymers, and it was therefore instructive to investigate their properties in order to understand better the nature of LC polymers. In general the isotropisation temperature for imines **PBBA1200X** was lower than for **PBBA470X** (see Table 3). This behaviour confirmed the influence of the length of the aliphatic chain on the thermal properties of these compounds.

PBBA1200B exhibited smectic mesophase behaviour, whereas in the case of **PBBA1200A** only a crystal–isotropic transition was observed. It was found that the presence of fluorinated chains promoted the appearance of LC properties, as in **PBBA1200B**, by comparison with **PBBA1200A** which contained no fluorinated chains. Moreover, increasing the length of the aliphatic element in a rod-like azomethine is accompanied by a reduction in mesomorphic behaviour (compare **PBBA1200A** and **PBBA470C**). Figure 7 shows microphotographs of the textures of selected examples.

During cooling **PBBA470D** from the isotropic phase to room temperature crystallisation was not observed (Figure 7(b)). The optical texture of **PBBA1200A** observed at 59°C and after cooling from the isotropic phase to room temperature was similar (Figure 7(c) and (d)) and X-ray assessment did not reveal LC behaviour (see the following section**)**. On the other hand, during cooling **PBBA1200A** from the isotropic phase to room temperature, crystallisation was observed (Figure 7(d)).

Condensation of the appropriate monoaldehyde with diamines thus leads to thermotropic π-conjugated calamitic B–A–B triblock compounds (**PBBA470A**, **PBBA470C**, **PBBA1200A**) or C–B–A–B–C pentablock LC compounds (**PBBA470D** and **PBBA1200B**), as shown in Figure 8.

In the case of LC dimers, it has been shown that for smectic behaviour to be observed the length of the terminal chains is required to exceed half the spacer length [36]. We did not observe this, however. In the present case, **PBBA470C** exhibited smectic phases, but imine **PBBA1200A** did not. Our preliminary proposal is that in these compounds specific interactions between the ether oxygen atoms along the spacer are responsible for driving the formation of the smectic phase.

Moreover, smectic phase formation in **PBBA1200B** arises from the lack of compatibility between perfluoro chains, aromatic units and flexible spacers. Such behaviour has been observed in azomethine diimides obtained from a similar aldehyde containing a fluorinated chain [37].

Our experiments show the strong influence of the length of the flexible segments in the core, and the nature of the terminal chains, on the LC properties of these azomethines.

2.5 X-ray diffraction (XRD) measurements

XRD studies on **PBBA1200B** revealed a two-stage melting process. Patterns recorded at room temperature (Figures 9(a) and 9(d)) were characteristic of a crystalline phase, and contained a number of incommensurate Bragg reflections in the low- and high-angle regions. On the other hand, the pattern obtained at 100°C (Figure 9(c)) contained no sharp signals, pointing to the absence of the long-range order typical of an isotropic liquid. At 80°C, however, the pattern obtained (Figures 9(b), (d) and (e)) was characteristic of a LC smectic phase, and contained a series of sharp commensurate signals in the low-angle region arising from long-range one-dimensional density modulation (layers) and a diffuse signal indicating no ordering in the layers, and an intermolecular distance of about 4.5 Å. The smectic periodicity of **PBBA1200B** was 61.9 Å at 80°C.

In a previous study we have investigated the azomethine **PBBA470C** by XRD [35], and showed that it formed two smectic phases, SmA and SmB. The lower temperature phase was identified as hexatic smectic B phase. In the crystalline phase a doubling of the basic layer periodicity was found, evidenced by the appearance of subharmonics in the main small-angle signal.

The XRD studies performed on **PBBA470A, PBBA470D and PBBA1200A** at room temperature

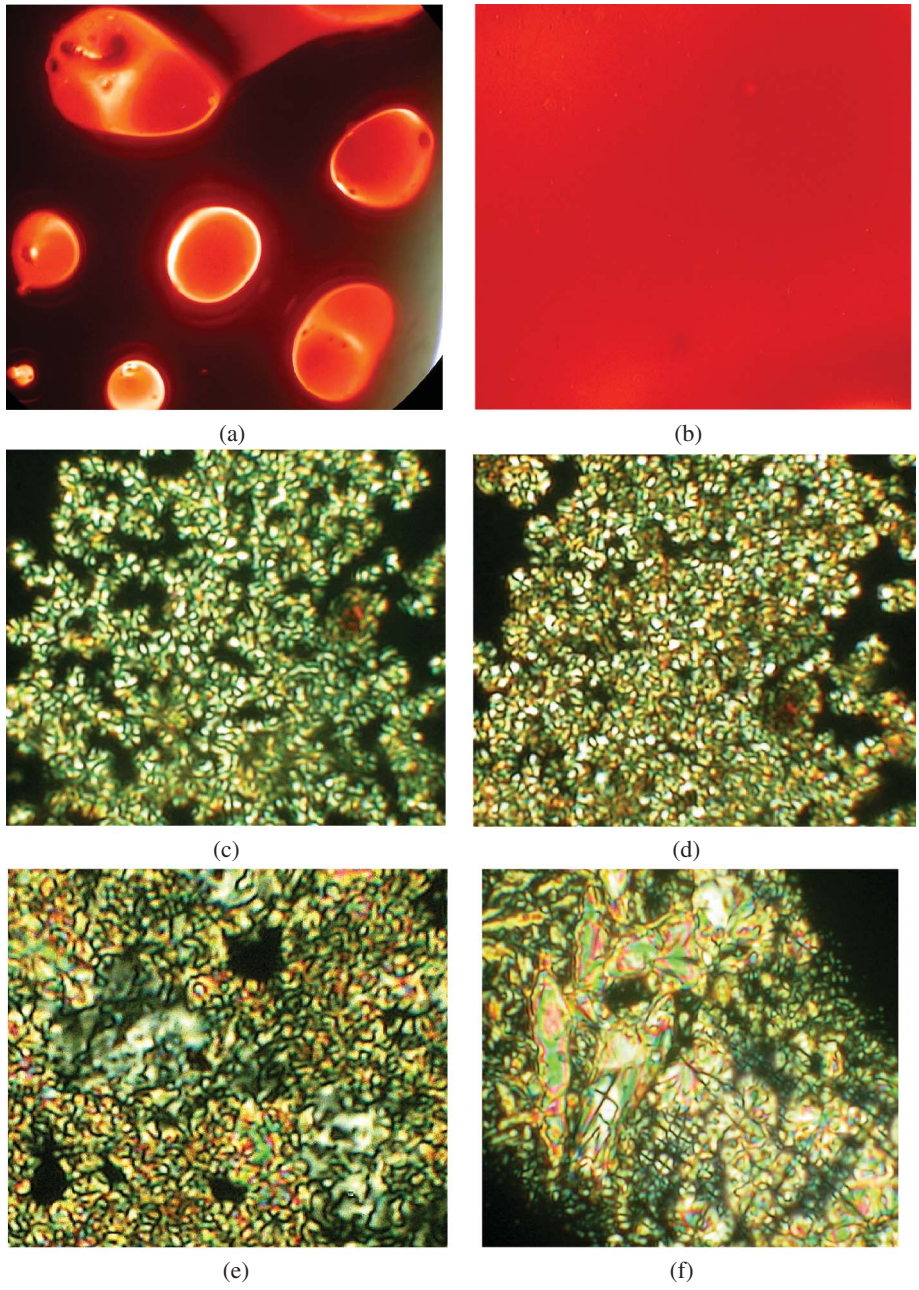

Figure 7. Photomicrographs of the optical textures of (a) **PBBA470D** (at 87.60°C), (b) **PBBA470D** (after cooling from the isotropic state to room temperature), (c) **PBBA1200A** (at 59.00°C), (d) **PBBA1200A** (at 25.00°C), (e) **PBBA1200B** (at 81.40°C) and (f) **PBBA1200B** (at 106.00°C).

revealed that all these compounds were in the isotropic liquid phase (Figure 10).

3. Conclusions

The (opto)electrical and mesomorphic properties of two series of dimeric molecules are described in which the imine groups are linked to an oxyalkylene spacer by phenylene rings and ester groups. In order to study the relationships between structure and properties, the length of the oxyalkylene spacers (3 or 12 units), as well as the nature of the terminal chains, has been varied. The results show that both the spacer and terminal groups have an impact on the mesomorphic behaviour of the imines. Novel symmetrical imines have been synthesised and characterised by NMR, FTIR and UV–Vis spectroscopy, and by *I–V*, DSC, POM and AFM.

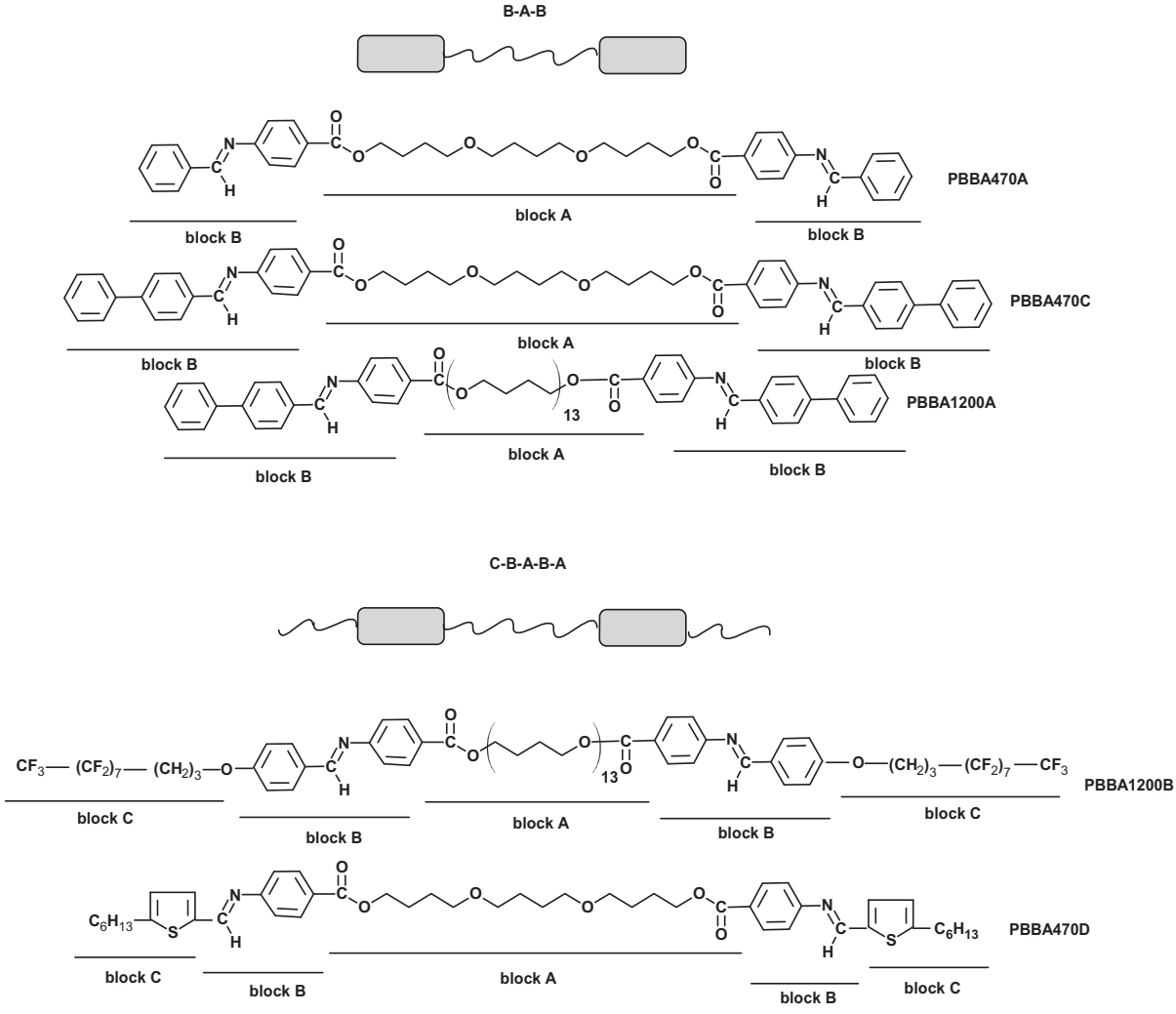

Figure 8. Schematic presentation of the azomethines as triblock (B–A–B) or pentablock (C–B–A–B–A) compounds.

4. Experimental

4.1 Materials

All chemicals and reagents were obtained from Aldrich and used as received.

*4.1.1 Synthesis of imines from **PBBA470***

Poly(1,4-butanediol)bis(4-aminobenzoate) (1 mmol) and the relevant aldehyde (2 mmol) were mixed in a glass reactor provided with stirrer. The reaction mixture was purged with nitrogen for 30 min and the temperature raised to 170°C for 24 h under an atmosphere of nitrogen. The mixture was cooled to room temperature and the solid matter scraped together and powdered. The crude product was washed three times with methanol and twice further with acetone, to remove unreacted diamine and aldehyde. The product was finally dried at 60°C for 24 h under vacuum and characterised by thin-layer chromatography (TLC) (eluent, dichloroethane/ethyl acetate, 50/50). Analytical TLC was performed on silica gel plates (F_{254}, Merck).

PBBA470A: 4,4′-(butane-1,4-diylbis(oxy)bis(butane-4,1-diyl) bis(4-(phenyl-4-ylmethyleneamino)benzoate)

^{1}H NMR (300 MHz, $CDCl_3$, TMS) [ppm] δ: 8.45 (s, 2H, C**H**=N), 8.05–8.15 (d, 4H, 2 × $\mathbf{H}_{Ar}$–C(O)O), 7.83–7.86 (m, 4H, 2 × $\mathbf{H}_{Ar}$–CH), 7.20–7.40 (m, 6H, 2 × $\mathbf{H}_{Ar}$), 6.61–6.65 (m, 4H, 2 × $\mathbf{H}_{Ar}$–N), 4.26 (m, 4H, 2 × C**H**$_2$–C(O)O), 3.44–3.48 (m, 8H, 4 × C**H**$_2$–O), 1.63–1.74 (m, 12H, (C**H**$_2$)$_6$).
^{13}C NMR (75 MHz, $CDCl_3$, TMS) [ppm] δ: 166.67 (–**C**(O)O–), 150.71 (**C**H=N), 134.46, 131.88, 131.56, 130.83, 129.74, 129.04, 128.99, 128.85, 120.64, 120.00, 113.75, 77.42, 77.19, 77.00, 76.57, 70.67, 70.59, 70.27, 64.17, 26.88, 26.48, 26.40, 25.68, 25.25, 14.11.

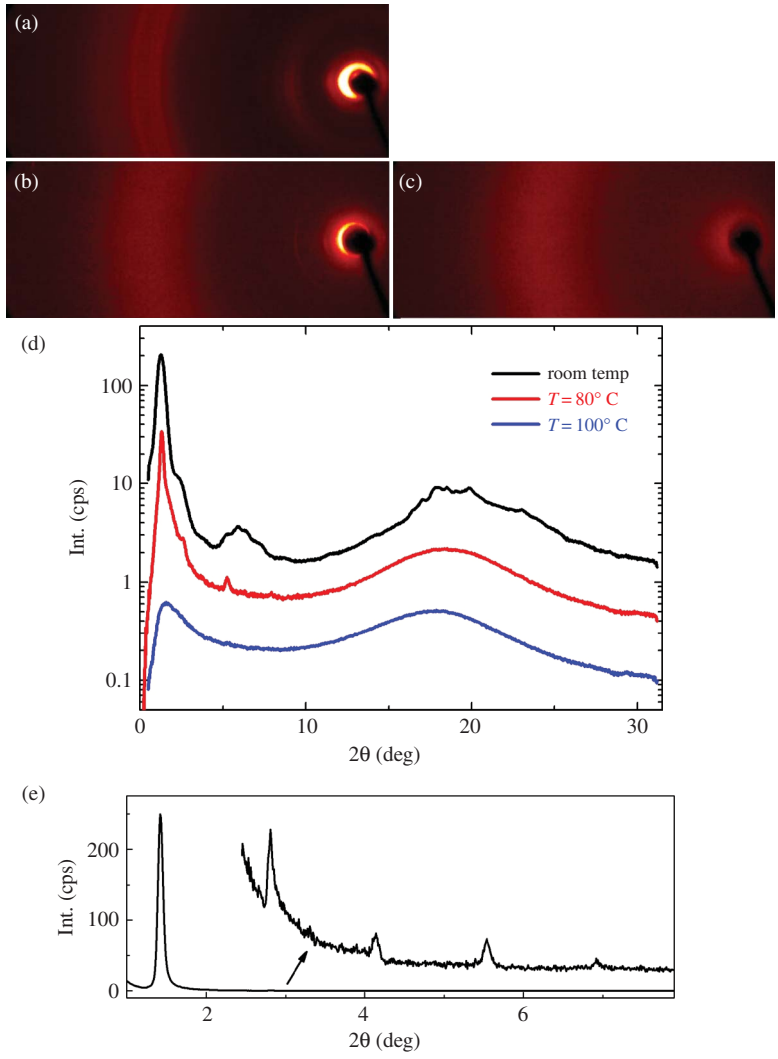

Figure 9. 2D XRD patterns obtained for **PBBA1200B** at (a) room temperature, (b) 80°C and (c) 100°C. (d) Intensity of X-ray signal *vs* diffraction angle, obtained by integration of 2D patterns over azimuthal angle for **PBBA1200B**. For ease of presentation the curves are vertically shifted. (e) Small-angle XRD pattern obtained for a well aligned sample of **PBBA1200B** at 80°C (measurement in reflection mode), showing a series of five commensurate Bragg-type signals indicating well defined smectic layers (colour version online).

ν_{max} (KBr)/cm^{-1}: 3459, 3363, 3241, 2945, 2863, 2799, 1695, 1627, 1603, 1518, 1468, 1447, 1384, 1310, 1274, 1172, 1108, 957, 844, 772, 699.

T_g (°C): −7.0.

PBBA470B: 4,4′-(butane-1,4-diylbis(oxy)bis(butane-4,1-diyl)bis(4-(hydroxyphenyl-4-ylmethyleneamino) benzoate)

^{1}H NMR (300 MHz, $CDCl_3$, TMS) [ppm]: insoluble in chloroform.

ν_{max} (KBr)/cm^{-1}: 3226, 2947, 2866, 2841, 1704, 1620, 1601, 1513, 1460, 1384, 1273, 1170, 1098, 952, 839, 769.

T_g (°C): 23.5.

PBBA470C: 4,4′-(butane-1,4-diylbis(oxy)bis(butane-4,1-diyl)bis(4-(biphenyl-4-ylmethyleneamino)benzoate)

^{1}H NMR (300 MHz, $CDCl_3$, TMS) [ppm] δ: 8.47 (s, 2H, 2 × C**H**=N), 8.07–8.10 (d, 4H, 2 × $\mathbf{H}_{Ar}$–O–C=O), 7.97–7.99 (d, 4H, 2 × $\mathbf{H}_{Ar}$–CH), 7.64–7.74 (m, 8H, 4 × $\mathbf{H}_{Ar}$), 7.45–7.50 (m, 2H, 2 × $\mathbf{H}_{Ar}$), 7.30–7.39 (m, 4H, 2 × $\mathbf{H}_{Ar}$), 7.24–7.26 (m, 4H, 2 × $\mathbf{H}_{Ar}$–N), 4.36 (m, 4H, 2 × C$\mathbf{H}_2$–O–CO), 3.46–3.51 (m, 8H, 4 × C$\mathbf{H}_2$–O), 1.64–1.87 (m, 12H, (C$\mathbf{H}_2$)$_6$).
^{13}C NMR (75 MHz, $CDCl_3$, TMS) [ppm] δ: 166.37 (–O–**C**O), 161.19 (**C**H=N), 156.19, 144.56, 140.09, 134.70, 131.55, 130.84, 130.27, 129.53, 129.00, 128.92, 128.46, 128.02, 127.68, 127.62, 127.50, 127.35, 127.18, 120.69, 113.74, 77.42, 77.20, 77.00,

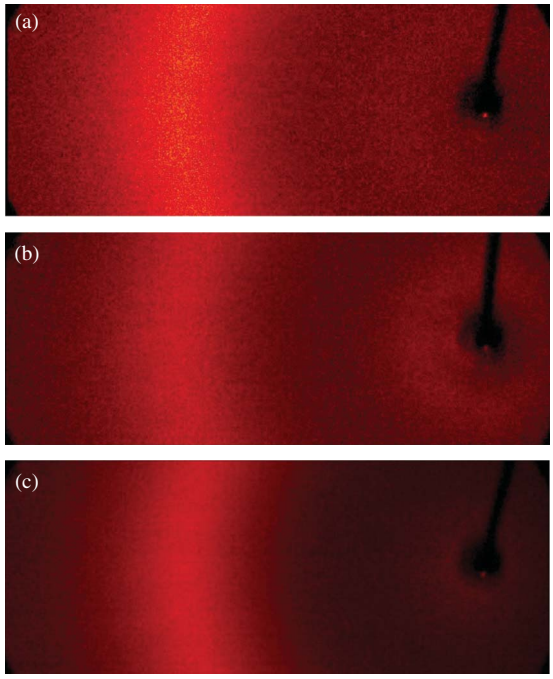

Figure 10. 2D X-ray patterns of (a) **PBBA470A**, (b) **PBBA470D** and (c) **PBBA1200A**, observed at room temperature, all in the isotropic liquid phase.

76.58, 70.72, 70.35, 70.24, 64.79, 64.16, 26.49, 26.39, 25.66.

ν_{max} (KBr)/cm^{-1}: 3034, 2939, 2861, 2804, 1718, 1711, 1625, 1594, 1581, 1561, 1486, 1471, 1450, 1411, 1375, 1363, 1338, 1306, 1286, 1250, 1209, 1169, 1123, 1099, 1006, 972, 891, 853, 833, 771, 759, 732, 719, 688, 557, 532.

UV–Vis (nm): 311. **T_g** (°C): 23.8.

PBBA470D: 4,4′-(butane-1,4-diylbis(oxy)bis(butane-4,1-diyl)bis(4-(5-hexylthiophene-2-ylmethleneamino) benzoate))

^{1}H NMR (300 MHz, $CDCl_3$, TMS) [ppm] δ: 8.57 (m, 2H, 2 × C**H**=N), 8.10 (m, 4H, 2 × **H**$_{Ar}$–C(O)O), 7.80 (m, 2H, 2 × C**H** [thiophen]), 7.10–7.30 (m, 4H, **H**$_{Ar}$–N), 6.60 (m, 2H, 2 × C**H** [thiophen]), 4.20–4.50 (m, 4H, 2 × C**H**$_2$–C(O)O), 3.44–3.46 (m, 8H, 4 × C**H**$_2$–O), 2.80–3.00 (m, 4H, 2 × C**H**$_2$–thiophen), 1.68–1.74 (m, 4H, 2 × C**H**$_2$–CH_3), 1.27–1.34 (m, 24H, 2 × (C**H**$_2$)$_3$ [thiophen] and (C**H**$_2$)$_6$), 0.83–0.98 (m, 6H, 2 × C**H**$_3$),

^{13}C NMR (75 MHz, $CDCl_3$, TMS) [ppm] δ: 166.00 (–**C**(O)O–), 153.50 (**C**H=N), 131.01, 112.60, 69.75, 69.48, 40.33, 40.05, 39.77, 39.49, 39.21, 38.94, 38.66, 34.17, 30.96, 26.32, 26.05, 25.92, 25.39, 13.90.

ν_{max} (KBr)/cm^{-1}: 3458, 3365, 3241, 3067, 2952, 2920, 2851, 1711, 1604, 1592, 1518, 1463, 1411, 1376, 1308, 1269, 1168, 1108, 958, 854, 802, 770.

UV–Vis (nm): 304. **T_g** (°C): −11.7.

*4.1.2 Synthesis of imines from **PBBA1200***

The method was exactly similar to that described for imines from **PBBA470,** *4.1.1*, above.

PBBA1200A: bis [4- ((4-biphenylomethyleno) amino) benzoate] 29,29′- [(butylo-1,4-diylbis(oxy))bis(5,10,15, 20,25-pentaoxynonacozane)]

^{1}H NMR (300 MHz, $CDCl_3$, TMS) [ppm] δ: 8.48 (s, 2H, 2 × C**H**=N), 8.07 (d, 4H, 2 × **H**$_{Ar}$–C(O)O), 7.97 (d, 4H, 2 × **H**$_{Ar}$–CH), 7.83 (d, 4H, 2 × **H**$_{Ar}$), 7.40–7.74 (m, 10H, 2 × **H**$_{Ar}$), 7.22–7.25 (m, 4H, 2 × **H**$_{Ar}$–N), 4.26–4.38 (m, 4H, 2 × C**H**$_2$–C(O)O), 3.41 (m, 48H, 24 × C**H**$_2$–O), 1.62–1.86 (m, 52H, (C**H**$_2$)$_{26}$).

^{13}C NMR (75 MHz, $CDCl_3$, TMS) [ppm] δ: 166.65 (–**C**(O)O–), 161.17 (**C**H=N), 156.16, 150.75, 144.54, 140.05, 134.67, 131.52, 130.81, 130.24, 129.51, 128.97, 128.89, 128.41, 128.00, 127.65, 127.48, 127.32, 127.16, 120.66, 119.87, 113.69, 83.98, 81.65, 77.42, 77.00, 76.57, 70.56, 64.77, 64.14, 26.44, 25.64.

ν_{max} (KBr)/cm^{-1}: 3361, 3243, 2943, 2919, 2863, 2801, 1709, 1626, 1605, 1561, 1519, 1486, 1448, 1410, 1373, 1309, 1273, 1210, 1171, 1114, 1002, 996, 964, 891, 824, 771, 759, 699.

UV–Vis (nm): 275. **T_g** (°C): −51.9.

PBBA1200B: bis[4-(4-(4,4,5,5,6,6,7,7,8,8,9,9,10,10,11, 11,11-heptadecafluoroundecyloxy) benzylidenoamino) benzoate] 29,29′-[(butylo-1,4-diylbis(oxy))bis (5,10,15, 20,25-pentaoxynonacozane)]

^{1}H NMR (300 MHz, $CDCl_3$, TMS) [ppm] δ; 8.37 (s, 2H, 2 × C**H**=N), 8.05–8.08 (d, 4H, 2 × **H**$_{Ar}$–C(O)O), 7.84–7.88 (m, 4H, 2 × **H**$_{Ar}$–CH), 7.18–7.20 (d, 4H, 2 × **H**$_{Ar}$–N), 6.98–7.01 (d, 4H, 2 × **H**$_{Ar}$–O), 4.26–4.36 (m, 4H, 2 × C**H**$_2$–C(O)O), 4.11–4.14 (m, 4H, 2 × C**H**$_2$–O–Ph), 3.42 (m, 48H, 24 × C**H**$_2$–O), 2.16–2.35 (m, 8H, 2 × (C**H**$_2$)$_2$–CF_2), 1.62–1.81 (m, 52H, (C**H**$_2$)$_{26}$).

^{13}C NMR (75 MHz, $CDCl_3$, TMS) [ppm] δ: 166.30 (–**C**(O)O–), 161.00 (**C**H=N), 156.50, 151.00, 131.54, 130.85, 120.67, 114.66, 113.72, 77.43, 77.00, 76.58, 70.58, 70.52, 64.16, 26.46, 25.66.

ν_{max} (KBr)/cm^{-1}: 3366, 3246, 2941, 2919, 2853, 2799, 1710, 1626, 1605, 1576, 1513, 1472, 1440, 1413, 1372, 1333, 1310, 1274, 1252, 1210, 1170, 1146, 1115, 1024, 854, 822, 772.

UV–Vis (nm): 274. **T_g** (°C): −60.2.

4.2 Instrumental

The compounds synthesised were characterised by ^{1}H and ^{13}C NMR and FTIR spectroscopy. NMR results were recorded on a Bruker AC 300 MHz. Deuterated chloroform ($CDCl_3$) containing tetramethylsilane (TMS) as internal standard was used as solvent. FTIR spectra of the compounds were recorded on a Perkin–Elmer Paragon 500 spectrometer (absorption range, 400–4000 cm^{-1}; resolution, 2 cm^{-1}).

I–V measurements were carried out using an ITO/compound/Alq_3/Al device. The azomethine solution (1 w/v % in dichloroethane) was spin-cast on an ITO-covered glass substrate at room temperature. Residual solvent was removed by heating the film under vacuum. The Alq_3 layer was prepared on the surface of the compound film by vacuum deposition at 2×10^{-4} Pa, and the Al electrode was vacuum deposited at a similar pressure. The area of the diodes was 9 mm^2. *I–V* characteristics were determined using a Keithley 6715 electrometer.

The phase transitions and mesogeneity were studied by DSC and POM. DSC studies were conducted on a TA DSC 2010 (TA Instruments, New Castle, DE) under a nitrogen atmosphere using sealed aluminium pans. The textures of the LC phase were observed under a POM Zeiss Opton–Axioplan equipped with a Nikon Coolpix 4500 digital colour camera, and a Mettler FP82 hot-plate provided with Mettler FP80 temperature controller.

Two dimensional wide-angle XRD patterns were recorded at various temperatures on a Bruker D8 GADDS diffractometer (parallel point beam of CuKα radiation formed by Goebel mirror and point collimator, HiStar area detector). The samples were prepared as droplets on the heated plate.

UV–Vis absorption spectra were recorded in the solid state as films cast on quartz, using a Jasco V670 spectrophotometer. The quartz substrates were purified using organic solvents such as chloroform and acetone.

The surface morphology investigation of the compounds was performed in air using a commercial Innova AFM system from Veeco. Measurements were carried out in tapping mode by phase imaging. Local contrast data processing was also used. A typical cantilever of about 40 N m^{-1} and less than 10 nm tip curvature was employed.

Acknowledgements

The authors are grateful to Dr Patrice Rannou for kindly supplying **PBBA470** and **PBBA1200**. Mr M. Domanski carried out the *I–V*, Dr B. Kaczmarczyk the FTIR, and Mrs K. Zbikowska the NMR measurements.

References

[1] Goodby, J.W.; Saez, I.M.; Cowling, S.J.; Gasowska, J.S.; MacDonald, R.A.; Sia, S.; Watson, P.; Toyne, K.J.; Hird, M.; Lewis, R.A.; Lee, S.E.; Vaschenko, V. *Liq. Cryst*. **2009**, *36*, 567–605.
[2] Imrie, C.T.; Henderson, P.A.; Yeap, G.Y. *Liq. Cryst*. **2009**, *36*, 755–777.
[3] Imrie, C.T.; Henderson, P.A. *Chem. Soc. Rev*. **2007**, *36*, 2096–2124.
[4] Yoshizawa, A. *J. Mater. Chem.* **2008**, *18*, 2877–2889.
[5] Imrie, C.T.; Henderson, P.A. *Curr. Opin. Colloid Interface Sci*. **2002**, *7*, 298–311.
[6] Ferrarini, A.; Greco, C.; Luckhurst, G.R. *J. Mater. Chem*. **2007**, *17*, 1039–1042.
[7] Aziz, N.; Kelly, S.M.; Duffy, W.; Goulding, M. *Liq. Cryst*. **2008**, *35*, 1279–1292.
[8] Srivastava, R.M.; Filho, R.A.W.N.; Schneider, R.; Vieira, A.A.; Gallardo, H. *Liq. Cryst*. **2008**, *35*, 737–742.
[9] Toh, C.L.; Xu, J.; Lu, X.; He, C. *Liq. Cryst*. **2008**, *35*, 241–251.
[10] Bai, B.; Wang, H.; Zhang, P.; Qu, S.; Li, F.; Yu, Z.; Long, B.; Li, M. *Liq. Cryst*. **2008**, *35*, 793–798.
[11] Wang, H.; Shao, R.; Zhu, C.; Bai, B.; Gong, C.; Zhang, P.; Li, F.; Li, M.; Clark, N.A. *Liq. Cryst*. **2008**, *35*, 967–974.
[12] Centore, R. *Liq. Cryst*. **2009**, *36*, 239–245
[13] Bialecka-Florjanczyk, E.; Sledzinska, I.; Gorecka, E.; Przedmojski, J. *Liq. Cryst*. **2008**, *35*, 401–406.
[14] Bhowmik, P.K.; Han, H.; Nedeltchev, A.K.; Mandal, H.D.; Jimenez-Hernandez, J.A.; McGannon, P.M.; Lopez, L.; Kang, S.W.; Kumar, S. *Liq. Cryst*. **2009**, *36*, 1389–1399.
[15] Henderson, P.A.; Imrie, C.T. *Macromolecules* **2005**, *38*, 3307–3311.
[16] Henderson, P.A.; Inkster, R.T.; Seddon, J.M.; Imrie, C.T. *J. Mater. Chem*. **2001**, *11*, 2722–2731.
[17] Henderson, P.A.; Imrie, C.T. *Liq. Cryst*. **2005**, *32*, 1531–1541.
[18] Marcelis, A.T.M.; Giesbers, M.; Koudijs, A. *Liq. Cryst*. **2007**, *34*, 811–817.
[19] Aldred, M.P.; Hudson, R.; Kitney, S.P.; Vlachos, P.; Liedtke, A.; Woon, K.L.; O'Neill, M.; Kelly, S.M. *Liq. Cryst*. **2008**, *35*, 413–427.
[20] Guo, J.; Sun, J.; Li, K.; Cao, H.; Yang, H. *Liq. Cryst*. **2008**, *35*, 87–97.
[21] Gupta, V.K.; Sharma, R.K.; Mathews, M.; Yelamaggad, C.V. *Liq. Cryst*. **2009**, *36*, 339–343.
[22] Cong, Y.H.; Wang, W.; Tian, M.; Meng, F.B.; Zhang, B.Y. *Liq. Cryst*. **2009**, *36*, 455–460.
[23] Zhan, X.; Jing, X.; Wu, C. *Liq. Cryst*. **2009**, *36*, 1349–1354.
[24] Zhang, C.; Jin, L.; Yin, B.; Jamil, M.; Jeon, Y.J. *Liq Cryst*. **2008**, *35*, 39–44.
[25] Sharma, R.K.; Gupta, V.K.; Mathews, M.; Yelamaggad, C.V. *Liq. Cryst*. **2008**, *35*, 1161–1167.
[26] Pandey, A.S.; Dhar, R.; Pandey, M.B.; Achalkumar, A.S.; Yelamaggad, C.V. *Liq. Cryst*. **2009**, *36*, 13–19.
[27] Sharma, R.K.; Gupta, V.K.; Mathews, M.; Yelamaggad, C.V. *Liq. Cryst*. **2009**, *36*, 225–230.
[28] Iwan, A.; Janeczek, H.; Rannou, P. *Spectrochim. Acta, Part A* **2009**, *72*, 72–81.
[29] Iwan, A.; Janeczek, H.; Jarzabek, B.; Rannou, P. *Materials* **2009**, *2*, 38–61.
[30] Iwan, A.; Janeczek, H.; Rannou, P.; Kwiatkowski, R. *J. Mol. Liq.* **2009**, *148*, 77–87.

[31] Iwan, A.; Janeczek, H.; Jarzabek, B.; Domanski, M.; Rannou, P. *Liq. Cryst.* **2009**, *36*, 873–883.
[32] Iwan, A.; Janeczek, H.; Domanski, M.; Rannou, P. *J. Mol. Liq.* **2010**, *151*, 30–38.
[33] Iwan, A.; Janeczek, H.; Kaczmarczyk, B.; Jarzabek, B.; Sobota, M.; Rannou, P. *Spectrochim. Acta, Part A* **2010**, *75*, 891–900.
[34] Iwan, A.; Janeczek, H. *Mol. Cryst. Liq. Cryst.* **2010**, *518*, 99–106.
[35] Iwan, A.; Bilski, P.; Janeczek, H.; Jarzabek, B.; Rannou, P.; Sikora, A.; Pociecha, D.; Kaczmarczyk, B. *J. Mol. Struct.* **2010**, *963*, 175–182.
[36] Date, R.W.; Imrie, C.T.; Luckhurst, G.R.; Seddon, J.M. *Liq. Cryst*. **1992**, *12*, 203–238.
[37] Schab-Balcerzak, E.; Iwan, A.; Krompiec, M.; Siwy, M.; Tapa, D.; Sikora, A.; Palewicz, M. *Synth. Met.* **2010**; doi:10.1016/j.synthmet.2010.08.011.